Journal of
Materials Chemistry A

RSC Publishing

PAPER

View Article Online
View Journal | View Issue

Published on 30 October 2012. Downloaded by HeFei University of Technology on 15/10/2015 13:22:22.

Cite this: *J. Mater. Chem. A*, 2013, **1**, 1148

Tuning the p-type conductivity of ZnSe nanowires *via* silver doping for rectifying and photovoltaic device applications†

Li Wang,[ab] Min Lu,[b] Xiangan Wang,[b] Yongqiang Yu,[b] Xingzhi Zhao,[b] Peng Lv,[b] Hongwei Song,[b] Xiwei Zhang,[c] Linbao Luo,[b] Chunyan Wu,[b] Yan Zhang[b] and Jiansheng Jie*[c]

Received 27th September 2012
Accepted 30th October 2012

DOI: 10.1039/c2ta00471b

www.rsc.org/MaterialsA

Applications of one-dimensional (1D) semiconductor nanostructures in nanoelectronics and nano-optoelectronics rely on the ability to rationally tune their electrical transport properties. Here we report the synthesis of single-crystalline Ag-doped ZnSe nanowires (NWs) by using silver sulfide (Ag_2S) as the p-type dopant *via* a thermal evaporation method. The ZnSe:Ag NWs had the zinc blende structure with [1$\bar{1}$1] growth orientation. Significantly, the conductivities of the NWs could be tuned over 9 orders of magnitude by adjusting the Ag doping levels. Field-effect transistors (FETs) constructed from the ZnSe:Ag NWs verified their p-type nature with a hole concentration of up to 2.1×10^{19} cm^{-3}, which is the highest value achieved for p-type ZnSe nanostructures thus far. Schottky barrier diodes (SBDs) based on the ZnSe:Ag NW/ITO junctions exhibited remarkable rectifying behavior, with a rectification ratio of $>10^7$ and a small ideality factor of $\sim$1.29 at 320 K. Moreover, photovoltaic devices were fabricated from the ZnSe NW array/Si p–n heterojunctions by aligning the p-ZnSe NWs in a parallel fashion on a n-Si substrate. The device with a graphene top electrode showed a large fill factor (FF) of 61%, yielding a power conversion efficiency of $\sim$1.04%. The realization of p-type ZnSe NWs with tunable conductivity opens up opportunities for a host of high-performance nanoelectronic and nano-optoelectronic devices.

1 Introduction

In the past decade, fabrication and device applications of one-dimensional (1D) semiconductor nanostructures such as nanowires (NWs) and nanoribbons (NRs) have attracted considerable attention. Their distinctive properties arising from the quantum confinement effect have opened new opportunities for applications in future nanoelectronics and nano-optoelectronics.[1–3] Among various wide band-gap semiconductors, the II–VI group semiconductor zinc selenide (ZnSe), with a direct band-gap of $\sim$2.70 eV at room temperature, is regarded as one of the most promising materials for optoelectronic applications, including short wavelength emitters,[4] photovoltaics,[5] laser screens,[6] thin-film transistors,[7] and so on. ZnSe nanostructures have been intensively studied due to their excellent optical and optoelectronic properties, and a host of ZnSe nanostructures with diverse structures and morphologies such as NWs,[8] NRs,[9] nanotubes (NTs),[10] hierarchical structures,[11] and heterostructures[12] have been fabricated, and their great potential for laser and optoelectronic devices has been further exploited.[13,14]

The ability to rationally tune the electronic and optoelectronic properties of semiconductor nanostructures is vital to their device applications.[15] To this end, the technique of doping by introducing appropriate donor or acceptor impurities into the host lattice is one of the most efficient methods. The transport properties of nanostructures can be precisely controlled by adjusting the types as well as the concentrations of the doping elements. In contrast to IV or III–V group semiconductors,[16] II–VI group semiconductors usually suffer from the serious self-compensation effect,[17] and as a result, most of them show unipolar conduction behavior, *i.e.*, only n- or p-type doping could be achieved. This disadvantage impedes their practical applications in optoelectronic devices. However, recent studies on II–VI nanostructures, such as ZnS and ZnSe NWs/NRs, demonstrated that complementary doping, *i.e.*, both

[a]*Key Lab of Special Display Technology, Ministry of Education, Hefei University of Technology, Hefei, Anhui 230009, P. R. China*

[b]*School of Electronic Science and Applied Physics, Hefei University of Technology, Hefei, Anhui 230009, P. R. China*

[c]*Institute of Functional Nano & Soft Materials (FUNSOM) and Jiangsu Key Laboratory for Carbon-Based Functional Materials & Devices, Soochow University, Suzhou, Jiangsu 215123, P. R. China. E-mail: jsjie@suda.edu.cn; Fax: +86-512-65882846; Tel: +86-512-65881265*

† Electronic supplementary information (ESI) available: Schematic illustration of the experimental setup for p-ZnSe NWs synthesis; four-probe detection of a single p-ZnSe NW with Cu/Au electrodes; electron transfer characteristics of the Sample 2 and 3 NWs; optoelectronic characteristics of the nanoSBD; electrical measurements on the devices without p-ZnSe NW arrays; *I–V* curve of a single NW with graphene electrodes; *I–V* curves of a p-ZnSe NW measured before and after plasma treatment. See DOI: 10.1039/c2ta00471b

This journal is © The Royal Society of Chemistry 2013

Published on 30 October 2012. Downloaded by HeFei University of Technology on 15/10/2015 13:22:22.

n- and p-type doping, could be realized by carefully controlling the experimental conditions.[18–20] It is suggested that the high crystallinity as well as the more elastic lattice of the nanostructures might be responsible for the superior doping performance. To date, p-type doping in ZnSe nanostructures has been accomplished by substituting the Se^{2-} ions with group V elements such as bismuth (Bi) and arsenic (As).[20,21] On the other hand, it is known that group IA and IB elements, such as Ag, Cu, Na, and Li *etc.*, could also be potential p-type dopants by substituting for the Zn^{2+} ions in ZnSe. Since group I elements are non-toxic and low-cost, their use may further simplify the synthesis process, as well as improving the doping efficiency. Nevertheless, highly efficient group I element doping in ZnSe nanostructures remains a challenge and has been seldom studied so far.

Semiconductor nanostructures are important building blocks for nanodevice applications owing to their distinctive properties. It is well known that junctions, such as metal–semiconductor junctions (Schottky junctions) and semiconductor–semiconductor junctions (p–n junctions), have constituted the basis of functional devices. However, differing from films, which have planar structures and allow the fabrication of junctions by layer-by-layer deposition techniques, the construction of single- or multi-junctions of nanostructures is rather complicated because of the small size and random orientation of the nanostructures. Although superior performances are expected for the nanojunctions, relatively few works have been concerned with nanojunctions for device applications.[22] Herein, we report the synthesis of Ag-doped ZnSe NWs with tunable p-type conductivity by using silver sulfide (Ag_2S) as the acceptor dopant *via* a simple co-evaporation method. The p-type transport properties of the ZnSe:Ag NWs were systemically studied *via* the characterization of single-NW based field-effect transistors (FETs). Furthermore, nano-Schottky barrier diodes (SBDs) with excellent rectifying characteristics were fabricated from the p-ZnSe NW/indium tin oxide (ITO) Schottky junctions. By combining the p-type ZnSe NWs with an n-type Si substrate, we also developed a feasible method to construct ZnSe NW array/Si p–n heterojunctions. It was found that the photovoltaic performance of the heterojunctions could be remarkably enhanced by using graphene as a transparent top electrode. Our results demonstrate that the ZnSe NWs with tunable p-type conductivity should have important applications in nanoelectronic and nano-photovoltaic devices.

2 Experimental details

2.1 Synthesis and characterization of Ag-doped ZnSe NWs

Ag-doped ZnSe NWs were synthesized in a horizontal quartz tube furnace (inner diameter 50 mm, length 120 cm) *via* an *in situ* doping method using Ag_2S as the dopant (ESI, Fig. S1†). In a typical experiment, 0.25 g ZnSe powder (99.9%, Aldrich) was loaded into an alumina boat and placed at the center of the tube furnace. Several silicon wafers coated with 10 nm Au catalyst were then placed ~10 cm downstream from the ZnSe source. Another alumina boat loaded with 0.03 g Ag_2S powder (99.9%, Aldrich) was located upstream of the ZnSe source. The system was first purged twice with H_2 carrier gas (5% in Ar) and evacuated to a base pressure of 6×10^{-3} Pa. Then the carrier gas was introduced at a constant flow rate of 30 sccm, and the pressure in the tube was adjusted to 200 Torr. Thereafter, the furnace was heated to 1050 °C at a rate of 20 °C min^{-1}, and maintained at this temperature for 2 h. The temperature of the Si substrates was ~720 °C during the reaction, while the temperature of the Ag_2S source depended on its distance from the ZnSe source. After the system was cooled down to room temperature, the Si substrates were taken out of the furnace and a layer of bright yellow product could be observed on their surfaces. The Ag doping concentration was controlled by varying the evaporation temperature of the Ag_2S source. In our work, three samples with different doping levels were synthesized, which were marked as Sample 1, Sample 2 and Sample 3, corresponding to the different Ag_2S evaporation temperatures of ~520, ~720, and ~820 °C, respectively, during the experiment. Undoped ZnSe NWs, marked as Sample 0, were also synthesized for comparison under the same conditions except that no Ag_2S was used. The morphologies and structures of the as-synthesized ZnSe:Ag NWs were characterized by scanning electron microscopy (SEM, Sirion 200 FEG), high-resolution transmission electron microscopy (HRTEM, JEOL-2010), and X-ray diffraction (XRD, D-500 using Cu Kα radiation). The compositions of the NWs were analyzed by energy-dispersive X-ray spectroscopy (EDS, attached to the SEM) and X-ray photoelectron spectroscopy (XPS, Thermo ESCALAB 250).

2.2 Construction of FETs and SBDs based on individual Ag-doped ZnSe NWs

To assess the electrical properties of the ZnSe:Ag NWs, FETs were constructed based on individual ZnSe NWs (inset in Fig. 2(a)). ZnSe NWs were first dispersed on the SiO_2 (300 nm)/p^+-Si substrate with the desired density. The NW density was carefully controlled to ensure a large probability for the single NW devices. After that, Cu (4 nm)/Au (50 nm) source and drain electrodes, which exhibited excellent ohmic contact to the p-type ZnSe NWs (ESI, Fig. S2†), were defined by photolithography and a subsequent lift-off process. The degenerately doped Si substrate served as the global back gate electrode in the FET. To fabricate the SBDs (Fig. 3(a)), additional photolithography and lift-off processes were carried out to define the ITO Schottky contact between two adjacent Cu/Au electrodes. A pulsed laser deposition (PLD) system with a KrF excimer laser (Lambda Physik COMPexPro 102, 248 nm, 120 mJ, 5 Hz) was used to deposit the ITO film (thickness 40 nm).

2.3 Construction of ZnSe NW array/Si p–n heterojunctions

Besides the FETs and SBDs, photovoltaic devices based on ZnSe NW array/Si p–n heterojunctions were fabricated as well (Fig. 4). First, ZnSe:Ag NWs were dispersed on an n-type Si (0.005 Ω cm^{-1}) substrate in a parallel fashion *via* a contact printing method.[23] Polymethylmethacrylate (PMMA) with a thickness of ~200 nm was then spin-coated onto the substrate as the insulator layer. After baking in air at 100 °C for 10 min, PMMA was etched in oxygen plasma (10.5 W) for 2 min to ensure that the top half of

Published on 30 October 2012. Downloaded by HeFei University of Technology on 15/10/2015 13:22:22.

the ZnSe NWs were exposed. After that, Au (10 nm) electrodes with 2 mm diameter were evaporated onto the top of the PMMA layer using a shadow mask. To evaluate the effects of different electrodes, monolayer graphene films (5 mm × 5 mm) instead of the Au electrodes were also used and directly transferred onto the top of the PMMA layer. All the electrical measurements were carried on a semiconductor characterization system (Keithley 4200-SCS). Temperature-dependent electrical measurements were performed using a low-temperature system (Janis/CCS-350S). White light (0.35 mW cm^{-2}) from the optical microscope on a probe station was used as the light source for the detection of photovoltaic properties.

3 Results and discussion

3.1 Characterization of the Ag-doped ZnSe NWs

SEM examination in Fig. 1(a) reveals that the ZnSe:Ag NWs were clean and uniform, with diameters in the range of 50–300 nm and lengths ranging from tens of micrometers up to hundreds of micrometers. It is noted that only Zn and Se elements with molar ratio of ~49 : 51 could be detected from the EDS spectrum (Sample 3, inset in Fig. 1(a)). XPS investigations on the ZnSe:Ag NWs were further performed to determine their compositions. We note that no XPS signal from Ag element could be detected except for in Sample 3, in which two weak peaks located at 368 and 374 eV, corresponding to the Ag 3d core level, have appeared (Fig. 1(b)), indicating an Ag content of ~0.6 at% in the NWs. Although Ag_2S was used as the dopant source in the reaction, neither EDS nor XPS detection showed a trace of S in the NWs. It seems that the S vapor coming from the decomposed Ag_2S powder had been carried out of the system by the carrier gas, or just deposited in the high temperature zone by forming ZnS with the Zn vapor. XRD patterns of both the undoped and doped ZnSe NWs are illustrated in Fig. 1(c). All the diffraction peaks could be properly assigned to zinc blende ZnSe (JCPDS no. 37-1463), except the peaks coming from the Si substrate. As compared with the undoped sample, no obvious peak shift or widening can be observed in the doped ones, revealing the high phase purity and crystallinity of the NWs. In addition, the HRTEM image and the corresponding selected-area electron diffraction (SAED) pattern of the ZnSe:Ag NW reveal that the NWs are zinc blende single crystals with a $[1\bar{1}1]$ growth orientation (Fig. 1(d)).

3.2 Electrical transport properties of the Ag-doped ZnSe NWs

Electrical measurements on individual ZnSe:Ag NWs were performed to evaluate the doping effects of Ag on their transport properties. Fig. 2(a) and (b) depict the typical *I–V* curves of the undoped and doped NWs, respectively. A representative SEM image of a single NW device is also shown in the inset of Fig. 2(a). Notably, it is seen that the conductance of these samples strongly depends on the evaporation temperature of the Ag_2S source during the NW growth. The different Ag_2S source temperatures can induce varied doping levels in the NWs. The undoped ZnSe NW (Sample 0) has the lowest conductivity of $\sim 2.1 \times 10^{-9}$ S cm^{-1} among all the samples (Fig. 1(a)), while the conductivity increases dramatically to $\sim 1.08 \times 10^{-3}$, 7.4×10^{-2}, and 6.24 S cm^{-1} for Sample 1, 2, and 3 (Fig. 1(b)), respectively. This result suggests that the conductivity of the ZnSe NWs could be tuned in a wide range of about 9 orders of magnitude by adjusting the Ag doping level. Furthermore, by applying a gate voltage (V_g) on the p^+-Si substrate, the typical gate-dependent source–drain current (I_{ds}) *versus* source–drain voltage (V_{ds}) curves of the ZnSe NW (Sample 1) were measured under varied gate voltage (V_g) from +40 to −40 V with a step of −20 V (Fig. 2(c)). Fig. 2(d) shows the I_{ds}–V_g curve measured at fixed $V_{ds} = -1$ V. Significantly, the

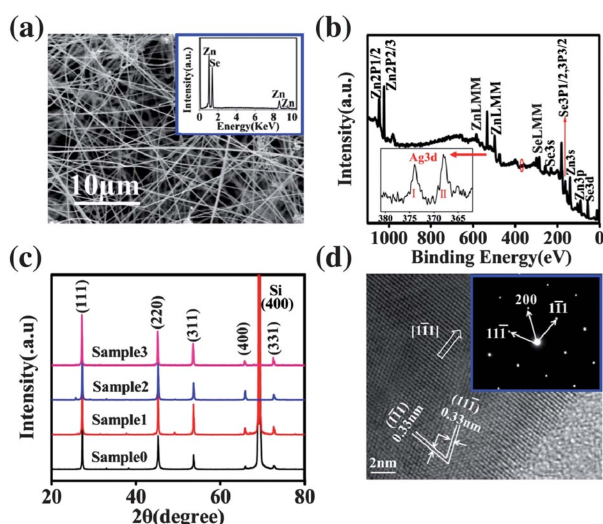

Fig. 1 Morphology and structure characterizations of the ZnSe:Ag NWs. (a) SEM image (Sample 3). Inset shows the EDS spectrum. (b) XPS spectrum (Sample 3). Inset shows the enlarged Ag 3d peaks. (c) XRD patterns of the samples with different doping levels. (d) HRTEM image (Sample 3). Inset shows the corresponding SAED pattern.

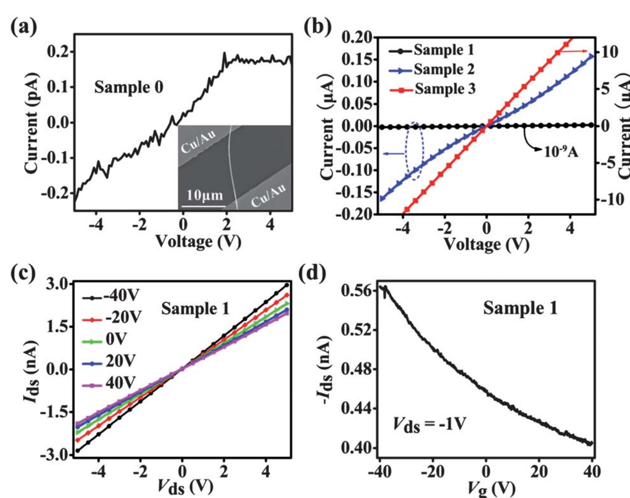

Fig. 2 (a) Typical *I–V* curve of an undoped ZnSe NW (Sample 0). Inset shows the top view SEM image of a single NW device. (b) Typical *I–V* curves of the Ag-doped ZnSe NWs with varied doping levels. (c and d) Electron transfer characteristics of the Ag-doped ZnSe NW (Sample 1). I_{ds}–V_{ds} curves were measured under different V_g ranging from +40 to −40 V with a step of −20 V. The I_{ds}–V_g curve was obtained at fixed $V_{ds} = -1$ V.

This journal is © The Royal Society of Chemistry 2013

Published on 30 October 2012. Downloaded by HeFei University of Technology on 15/10/2015 13:22:22.

device shows a pronounced gating effect, and negative I_{ds} increases with the decrease of V_g, which is the typical behavior of a p-channel metal-oxide–semiconductor FET (MOSFET), revealing that the ZnSe:Ag NWs are p-type semiconductors. Measurements on the NWs from Sample 2 and 3 also show similar results (ESI, Fig. S3†). This p-type characteristic originates from the substitutional doping of Ag^+ in the ZnSe NWs, replacing the Zn^{2+} ions. Hole mobility (μ_h) and concentration (n_h) of the ZnSe:Ag NWs can be further estimated according to the following equations:[24]

$$\mu_h = g_m \frac{\ln(4h/d)L}{2\pi\varepsilon_0\varepsilon_{SiO_2}V_{ds}} \quad (1)$$

$$n_h = \sigma/q\mu_h \quad (2)$$

where transconductance ($g_m = dI_{ds}/dV_g$) is extracted from the linear region of the I_{ds}–V_g curve. L is the channel length (15 μm), d is the NW diameter (average d is ~150 nm), ε_{SiO2} is the dielectric constant of the SiO_2 dielectric (~3.9), and h is the thickness of the SiO_2 dielectric (300 nm). Table 1 summarizes the electrical transport properties of the Ag-doped ZnSe NWs with various doping levels. It is found that the hole mobilities for Sample 1, 2, and 3 are 4.2×10^{-3}, 7.2×10^{-2}, and 1.9 $cm^2\ V^{-1}\ s^{-1}$, respectively. The increased hole mobility for the NWs with a higher doping level is likely attributed to the improved electrical contact.[25] Correspondingly, the hole concentrations are calculated to be 2.7×10^{18}, 6.4×10^{18}, and 2.1×10^{19} cm^{-3} for Sample 1, 2, and 3, respectively. We note that the hole concentration of 2.1×10^{19} cm^{-3} in this work represents the highest value achieved for p-type ZnSe nanostructures thus far,[20] indicating that the group I elements are very promising for realizing high-concentration p-type doping in II–VI nanostructures.

3.3 NanoSBDs based on p-ZnSe NW/ITO Schottky junctions

To exploit the potential applications of the p-type ZnSe NWs in nanoelectronic devices, p-ZnSe NW/ITO SBDs based on individual NWs were constructed. Fig. 3(a) shows the representative SEM image of the device. ITO was utilized since it has been widely used as a transparent electrode, and the use of it may facilitate the applications of the nanoSBDs in transparent and flexible electronics. From the room-temperature *I*–*V* characteristics shown in Fig. 3(b), it is clear that the nanoSBD exhibits excellent rectifying behavior with a low turn-on voltage of ~0.7 V and a high rectification ratio of >10^7. The reverse-bias breakdown is not observed up to −5 V. Fig. 3(c) depicts the temperature dependent rectifying characteristics of the nanoSBD. As

Table 1 Electrical transport properties of the Ag-doped ZnSe NWs with various doping levels

Sample no.	σ (S cm^{-1})	μ_h ($cm^2\ V^{-1}\ s^{-1}$)	n_h (cm^{-3})
1	1.08×10^{-3}	4.2×10^{-3}	2.7×10^{18}
2	7.4×10^{-2}	7.2×10^{-2}	6.4×10^{18}
3	6.24	1.9	2.1×10^{19}

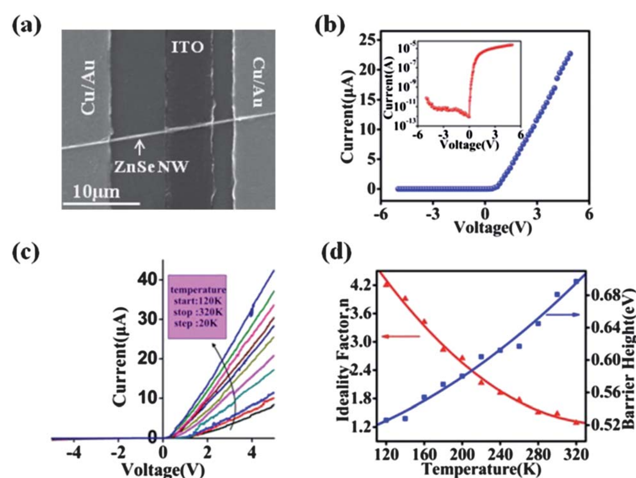

Fig. 3 (a) Typical SEM image of the nanoSBD fabricated from a single p-ZnSe NW. (b) Room-temperature rectifying characteristics of the nanoSBD. Inset shows the semi-logarithmic plot of the rectifying curve. (c) Rectifying characteristics of the nanoSBD measured at varied temperatures from 120 to 320 K. (d) Temperature dependence of the ideality factor and the barrier height of the nanoSBD.

the temperature increases from 120 to 320 K, the turn-on voltage tends to shift from 1.07 to 0.24 V, along with an increase of forward current. This device characteristic is in good agreement with that of a conventional Schottky device. The conduction current of a SBD is usually composed of thermionic emission current and tunnelling current. Assuming that the thermionic emission is the most predominant mechanism,[26] the rectifying characteristics of the nanoSBD can be described by the following equations:[24]

$$I = I_0\left[\exp\left(\frac{qV}{nkT}\right) - 1\right] \approx I_0 \exp\left(\frac{qV}{nkT}\right) \quad (3)$$

$$I_0 = AA^*T^2 \exp\left(-\frac{q\Phi_b}{kT}\right) \quad (4)$$

where I_0 is the reverse saturation current, n is the ideality factor, A is the area of Schottky contact, Φ_b is the Schottky barrier height, and A^* is the effective Richardson constant (72.02 A $cm^{-2}\ K^{-2}$ for ZnSe). Fig. 3(d) plots the relationship of n and Φ_b with temperature. It is found that n decreases from 4.20 to 1.29 when the temperature increases from 120 to 320 K, while Φ_b increased from 0.53 to 0.70 eV. We note that this analysis exhibits obvious deviations from the conventional Schottky theory, in which Φ_b should decrease with the increase of temperature. Similar phenomena have been investigated, for example, in a Au/n-Si Schottky barrier diode before, and the inhomogeneous barrier height was suggested as a reason for this deviation.[27] The electrons possess a weak kinetic energy at low temperatures, and they will prefer to pass through a low barrier, thus giving rise to a lower barrier height and a larger ideality factor at low temperatures.[27] Besides thermionic emission, it seems that tunnelling and leakage currents must be considered for precise estimation of the current transport in the p-ZnSe NW/ITO Schottky barrier.[28] Further analysis of the device characteristics of the nanoSBD is ongoing. On the other hand,

Published on 30 October 2012. Downloaded by HeFei University of Technology on 15/10/2015 13:22:22.

despite the obvious rectifying behavior, investigation of the optoelectronic characteristics of the nanoSBD under white light illumination (0.35 mW cm^{-2}) reveals a weak photoresponse (ESI, Fig. S4†). This result is likely attributed to the severe interface recombination as well as the relatively low light absorption of ZnSe NWs.

3.4 Photovoltaic devices based on p-ZnSe NW array/Si p–n heterojunctions

Due to the appropriate band-gap and strong absorption from blue to ultraviolet (UV) light, ZnSe shows great promise for photovoltaic applications.[5] In this work, we have conducted a preliminary study on ZnSe NW array/Si p–n heterojunctions and their photovoltaic characteristics. Fig. 4 illustrates the process for fabricating the heterojunctions, in which two kinds of electrodes, including Au (10 nm) and monolayer graphene film, are adopted as the top contact electrodes. From the optical images of the devices in Fig. 6(a) and (c), it can be seen that the p-ZnSe NWs are uniformly dispersed on the n-Si substrate and the NWs could be clearly viewed through the thin Au and graphene layers.

Prior to the measurement of the photovoltaic characteristics, surface potential microscopy (SPM) detection was performed to directly visualize the potential profile of the ZnSe NW/Si p–n heterojunction, as shown in Fig. 5. The topography of a single p-ZnSe NW on the n-Si substrate is displayed in Fig. 5(a). The upper image shows a 2D data plot of the topography with the corresponding colour bar, while in the lower graph a characteristic line measurement extracted from the 2D image is depicted. It can be seen that the NW has a diameter of ~70 nm. From the corresponding potential distribution in Fig. 5(b), the potential difference between the p-ZnSe NW and the n-Si substrate due to the equating Fermi levels is clearly visible in the upper image of the figure. The lower graph also shows the potential profile along the line, indicating a potential drop of ~30 mV between the p-ZnSe NW and the n-Si substrate. We note that this value is much lower than the theoretical built-in voltage of a ZnSe/Si p–n heterojunction under the same doping level, which can be as high as ~2.5 V based on the energy band alignment. This deviation could be explained in terms of the adsorption of surface contaminants such as water or oxygen, and the existence of surface states on the nanostructure.[29] In any case, the SPM measurement unambiguously reveals that a heterojunction has been formed between the p-ZnSe NW and the n-Si substrate.

Fig. 6(b) and (d) depict the photovoltaic characteristics of the ZnSe NW array/Si p–n heterojunctions measured with Au and graphene electrodes, respectively, under the white light (0.35 mW cm^{-2}) illumination from an optical microscope. We note that both the devices exhibit pronounced photovoltaic behavior. To clarify the origin of the photovoltaic behavior observed,

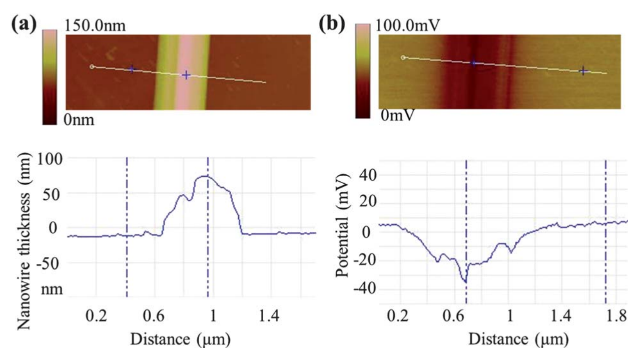

Fig. 5 (a) 2D measurement (top) and extracted line scan (bottom) of a topography measurement of a p-ZnSe NW on the n-Si substrate. (b) 2D measurement (top) and extracted line scan (bottom) of a potential measurement of the device.

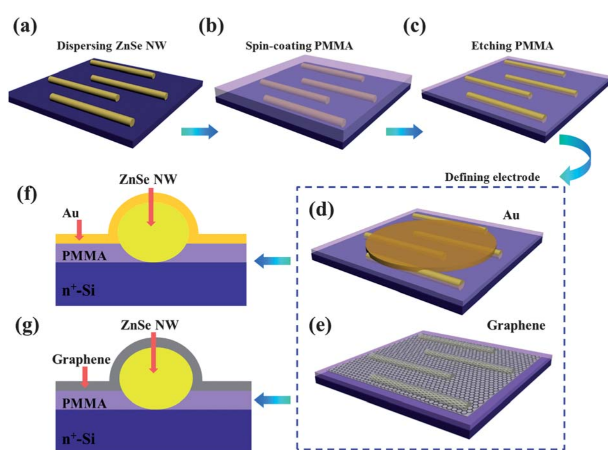

Fig. 4 Schematic illustration of the fabrication process of p-ZnSe NW array/Si p–n heterojunctions. (a) Parallel alignment of the p-ZnSe NWs on the n-Si substrate. (b) Spin-coating the PMMA insulator layer. (c) Etching the PMMA layer with O_2 plasma to expose the top half of the ZnSe NWs. (d) Defining Au top electrodes through a shadow mask. (e) Transferring monolayer graphene film onto the top of the PMMA layer as a transparent electrode. Cross-sectional views of the heterojunction devices with (f) Au top electrode and (g) graphene top electrode.

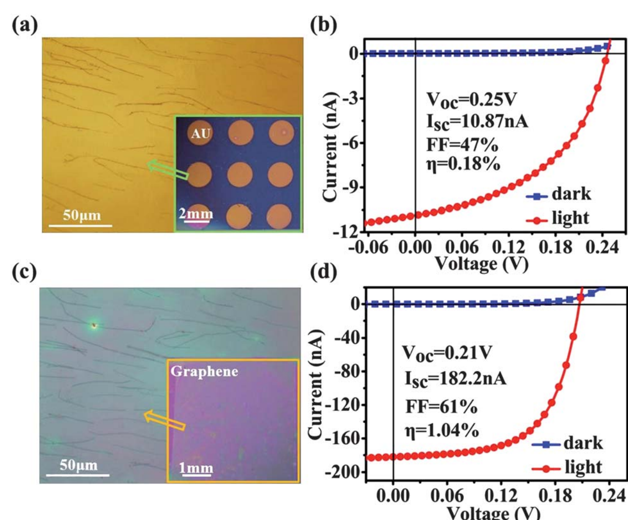

Fig. 6 Optical images of the parallel aligned NWs from the p-ZnSe NW array/Si p–n heterojunction photovoltaic devices with (a) Au electrodes and (c) monolayer graphene film electrodes. The insets show the low-magnification images of the devices. Photovoltaic characteristics of the devices with (b) Au electrodes and (d) graphene film electrodes under white light illumination.

This journal is © The Royal Society of Chemistry 2013

Published on 30 October 2012. Downloaded by HeFei University of Technology on 15/10/2015 13:22:22.

device counterparts fabricated by directly spin-coating PMMA onto a bare Si substrate were measured (ESI, Fig. S5†). It was found that no electrical signal could be detected in the devices without ZnSe NW arrays, indicating that the photovoltaic behaviors indeed come from the ZnSe NW array/Si p–n heterojunction. On the other hand, the conduction current of the p-ZnSe NW changes little upon the same plasma treatment (ESI, Fig. S7†). Therefore the influence of the plasma treatment on the device performance could be excluded. We note that the electrical properties of the p-ZnSe NWs are studied in the length direction in Fig. 2, whereas the photocurrent mainly travels along the direction perpendicular to the length of NWs in the heterojunction devices. Thus the anisotropic transport of nanostructures could be a potential factor that impacts the photovoltaic characteristics of the devices. However, considering the large diameter of the NWs, which is in the range of 50–300 nm and much higher than the Bohr radius of bulk ZnSe (4.1 nm),[30] this anisotropic effect should be very weak, and should not have a significant influence on the photovoltaic characteristics of the devices. Therefore the its impact is ignored in the following discussion.

The device with the Au electrode (Fig. 6(b)) possesses an open circuit voltage (V_{OC}) of 0.25 V, a short circuit current (I_{SC}) of 10.87 nA, and a fill factor (FF) of 47%, yielding a power conversion efficiency (η) of ~0.18%. Since only a small portion of the Si surface area was covered by the NWs, the junction area was estimated by first counting the average NW density on Si substrate (~200 NWs/300 × 300 μm^2), and then this value was multiplied by the average NW diameter (150 nm), the average NW length (80 μm), and the top electrode area. As we look at the device structure, the low transmittance (~80%) of the Au top electrode may prevent the full absorption of the incident light and thus limit the device performance. In contrast, graphene, which is an exciting new material for transparent electrode application, has a high optical transmittance (~97.7%) and large conductivity.[31,32] Electrical measurement of the single p-ZnSe NW with the graphene electrode shows good ohmic contact between the two (ESI, Fig. S6†), which means that graphene could serve as a high-performance transparent electrode in the ZnSe NW/Si heterojunction devices. As shown in Fig. 6(d), the device with the graphene top electrode shows much improved performance compared to the device counterpart with the Au electrode. V_{OC}, I_{SC}, FF can be estimated to be 0.21 V, 182.8 nA, and 61%, respectively, yielding a η value of ~1.04%. It is worth noting that the performance of the ZnSe NW array/Si heterojunction with the graphene electrode has surpassed many other nano-heterojunctions, such as p-Si/n-CdS/n-ZnO and Si/ZnO hierarchical nano-heterojunctions.[33–35] Also, the large FF (61%) for this device is seldom observed in nanophotovoltaic devices, which usually possess a small fill factor due to the strong interface recombination and the large contact resistance. The high-performance of the ZnSe NW array/Si heterojunction could be attributed to the high junction quality as well as the high transmittance/conductivity of the graphene electrode. Fig. 7(a) and (c) show the time response spectra of the heterojunctions measured under pulsed light illumination at zero external bias. The devices show excellent stability and reproducibility with a fast response time of less than 0.1 s (Fig. 7(b) and (d)), indicating that the photogenerated electron–hole pairs could be effectively separated and transported in the heterojunctions. The fast light response of the devices also makes them potential candidates for visible light detection.

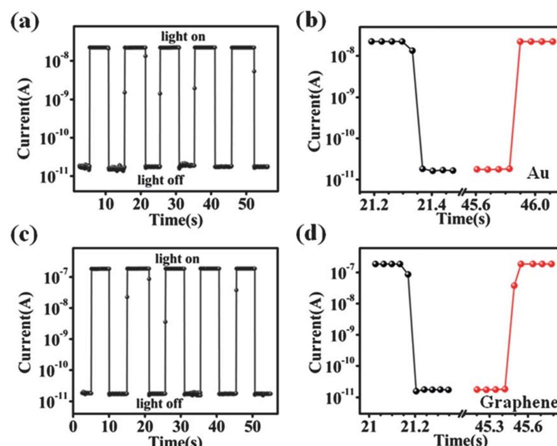

Fig. 7 Time response spectra of the devices with (a) Au electrodes and (c) graphene film electrodes measured at zero voltage bias under pulsed light illumination. The white light was turned on and off manually to generate the pulsed light. (b) and (d) show the enlarged rising and falling edges of the time response.

4 Conclusions

In summary, we first demonstrated that the group I element Ag could be a suitable dopant for achieving high-concentration p-type doping in ZnSe nanostructures. The conductivity of the ZnSe:Ag NWs could be tuned in a wide range of 9 orders of magnitude by adjusting the Ag doping level, giving rise to a hole concentration of up to 2.1×10^{19} cm^{-3}. NanoSBDs based on the ZnSe NW/ITO junction also exhibited excellent rectifying behaviors, with a rectification ratio of >10^7 and a small ideality factor of ~1.29 at 320 K. Moreover, we introduced a simple route to fabricate ZnSe NW array/Si p–n heterojunctions. By taking advantage of the highly transparent graphene as the top electrode, the photovoltaic performance of the heterojunction was dramatically enhanced, resulting in a large FF of 61% and a power conversion efficiency of up to ~1.04%. It is expected that the ZnSe NWs with tunable p-type conductivity should have important applications in future nanoelectronics and nano-optoelectronics.

Acknowledgements

This work was supported by financial support from the National Basic Research Program of China (2012CB932400, 2010CB301802), the Major Research Plan of the National Natural Science Foundation of China (no. 91027021, 91233110), the National Natural Science Foundation of China (no. 20901021, 51172151, 61106010, 21101051), the Foundation for Young Scientists in Higher Education Institutions of Anhui Province (no. 2011SQRL009ZD), and the Funds for the Excellent

Published on 30 October 2012. Downloaded by HeFei University of Technology on 15/10/2015 13:22:22.

Young Talents in Universities of the Education Department of Anhui Province (no. 2010AJYQ0360).

Notes and references

1 Y. Q. Bie, Z. M. Liao, H. Z. Zhang, G. R. Li, Y. Ye, Y. B. Zhou, J. Xu, Z. X. Qin, L. Dai and D. P. Yu, *Adv. Mater.*, 2011, **23**, 649.

2 G. Z. Shen, B. Liang, X. F. Wang, H. T. Huang, D. Chen and Z. L. Wang, *ACS Nano*, 2011, **5**, 6148.

3 G. Z. Shen, J. Xu, X. F. Wang, H. T. Huang and D. Chen, *Adv. Mater.*, 2011, **23**, 771.

4 T. Takahashi, T. Nakamura and S. Adachi, *Opt. Lett.*, 2009, **34**, 3923.

5 D. C. Perng, J. F. Fang and J. W. Chen, *J. Electrochem. Soc.*, 2011, **158**, H1097.

6 R. R. Alfano, Q. Z. Wang, T. Jimbo, P. P. Ho, R. N. Bhargava and B. J. Fitzpatrick, *Phys. Rev. A: At., Mol., Opt. Phys.*, 1987, **35**, 459.

7 J. Shah and A. E. DiGiovanni, *Appl. Phys. Lett.*, 1978, **33**, 995.

8 S. Y. Li, Y. Jiang, B. B. Wang, D. Wu, J. W. Li, Y. G. Zhang, B. Yang, X. N. Ding, H. Y. Zhou and H. H. Zhong, *Micro Nano Lett.*, 2011, **6**, 459.

9 Y. Jiang, X. M. Meng, W. C. Yiu, J. Liu, J. X. Ding, C. S. Lee and S. T. Lee, *J. Phys. Chem. B*, 2004, **108**, 2784.

10 B. Goswami, S. Pal, C. Ghosh and P. Sarkar, *J. Phys. Chem. C*, 2009, **113**, 6439.

11 F. Cao, W. D. Shi, L. J. Zhao, S. Y. Song, J. H. Yang, Y. Q. Lei and H. J. Zhang, *J. Phys. Chem. C*, 2008, **112**, 17095.

12 Z. M. Wu, Y. Zhang, X. A. Lin, X. H. Chen, B. W. Huang, H. Q. Wang, K. Huang, S. P. Li and J. Y. Kang, *J. Mater. Chem.*, 2011, **21**, 6020.

13 S. Gul, J. K. Cooper, C. Corrado, B. Vollbrecht, F. Bridges, J. H. Guo and J. Z. Zhang, *J. Phys. Chem. C*, 2011, **115**, 20864.

14 L. Wang, M. Lu, P. Lv, J. S. Jie, T. X. Yan, Y. Q. Yu, C. Y. Wu, Y. Zhang, C. Xie, P. Jiang, Z. Wang and Z. Z. Hu, *Sci. Adv. Mater.*, 2012, **4**, 332.

15 D. J. Chadi, *Phys. Rev. B: Condens. Matter Mater. Phys.*, 1999, **59**, 15181.

16 H. Morkoc, S. Strite, G. B. Gao, M. E. Lin, B. Sverdlov and M. Burns, *J. Appl. Phys.*, 1994, **76**, 1363.

17 D. B. Laks, C. G. Vandewalle, G. F. Neumark, P. E. Blochl and S. T. Pantelides, *Phys. Rev. B: Condens. Matter Mater. Phys.*, 1992, **45**, 10965.

18 Y. Q. Yu, J. S. Jie, P. Jiang, L. Wang, C. Y. Wu, Q. Peng, X. W. Zhang, Z. Wang, C. Xie, D. Wu and Y. Jiang, *J. Mater. Chem.*, 2011, **21**, 12632.

19 Q. Peng, J. S. Jie, C. Xie, L. Wang, X. W. Zhang, D. Wu and Y. Q. Yu, *Appl. Phys. Lett.*, 2011, **98**, 123117.

20 X. W. Zhang, J. S. Jie, Z. Wang, C. Y. Wu, L. Wang, Q. Peng, Y. Q. Yu, P. Jiang and C. Xie, *J. Mater. Chem.*, 2011, **21**, 6736.

21 H. S. Song, W. J. Zhang, G. D. Yuan, Z. B. He, W. F. Zhang, Y. B. Tang, L. B. Luo, C. S. Lee, I. Bello and S. T. Lee, *Appl. Phys. Lett.*, 2009, **95**, 033117.

22 Y. X. Chen, H. Gao and Y. Luo, *Appl. Phys. Lett.*, 2011, **99**, 143309.

23 T. Takahashi, P. Nichols, K. Takei, A. C. Ford, A. Jamshidi, M. C. Wu, C. Z. Ning and A. Javey, *Nanotechnology*, 2012, **23**, 045201.

24 L. Zhu, J. S. Jie, D. Wu, L. B. Luo, C. Y. Wu, Z. F. Zhu, Y. Q. Yu and L. Wang, *J. Nanoeng. Nanomanuf.*, 2012, **2**, 191.

25 Z. B. He, J. S. Jie, W. J. Zhang, W. F. Zhang, L. B. Luo, X. Fan, G. D. Yuan, I. Bello and S. T. Lee, *Small*, 2009, **5**, 345.

26 J. Appenzeller, M. Radosavljevic, J. Knoch and P. H. Avouris, *Phys. Rev. Lett.*, 2004, **92**, 048301.

27 R. Sharma, *J. Electron Dev.*, 2010, **8**, 286.

28 D. Donoval, A. Chvála, R. Šramatý, J. Kováč, E. Morvan, C. H. Dua, M. A. DiForte-Poisson and P. Kordoš, *J. Appl. Phys.*, 2011, **109**, 063711.

29 F. Robin, H. Jacobs, O. Homan, A. Stemmer and W. Bächtold, *Appl. Phys. Lett.*, 2000, **76**, 2907.

30 T. Miyajima, F. P. Logue, J. F. Donegan, J. Hegarty, H. Okuyama, A. Ishibashi and Y. Mori, *Appl. Phys. Lett.*, 1995, **66**, 180.

31 R. R. Nair, P. Blake, A. N. Grigorenko, K. S. Novoselov, T. J. Booth, T. Stauber, N. M. R. Peres and A. K. Geim, *Science*, 2008, **320**, 1308.

32 Y. Ye, Y. Dai, L. Dai, Z. J. Shi, N. Liu, F. Wang, L. Fu, R. M. Peng, X. N. Wen, Z. J. Chen, Z. F. Liu and G. G. Qin, *ACS Appl. Mater. Interfaces*, 2010, **2**, 3406.

33 W. Wang, Q. Zhao, K. Laurent, Y. Leprince-Wang, Z. M. Liao and D. P. Yu, *Nanoscale*, 2012, **4**, 261.

34 K. Sun, Y. Jing, N. Park, C. Li, Y. Bando and D. L. Wang, *J. Am. Chem. Soc.*, 2010, **132**, 15465.

35 W. Wang, Q. Zhao, J. Xu and D. P. Yu, *CrystEngComm*, 2012, **14**, 3015.

This journal is © The Royal Society of Chemistry 2013